Formation of $HCl^+(A^2\Sigma^+)$ and $HBr^+(A^2\Sigma^+)$ Resulting from $He(2^3S)$ Penning Ionization of HCl and HBr

Ikuo Tokue,* Hiroyuki Tanaka, and Katsuyoshi Yamasaki

Department of Chemistry, Faculty of Science, Niigata University, Ikarashi, Niigata 950-2181, Japan

Shinkoh Nanbu

Research Center for Computational Science, Okazaki National Research Institutes, Myodaiji, Okazaki 444-8585, Japan

Received: November 8, 2001; In Final Form: April 25, 2002

$He(2^3S)$ Penning ionization of HCl and HBr leading to $HCl^+(A)$ and $HBr^+(A)$ has been studied optically by using a crossed-beam apparatus. The ratios of the vibrational population, $P_{v'}/P_0$ ($v' = 2$ and 3) of $HCl^+(A)$ and P_1/P_0 of $HBr^+(A)$, increase with the collision energy in the region of 120−200 meV. The rotational distributions of $HCl^+(A, v'=0)$ and $HBr^+(A, v'=0)$ can be represented by a double-Boltzmann distribution; the temperatures are 200 ± 50 and 700 ± 80 K for $HCl^+(A, v'=0)$ and 250 ± 50 and 1200 ± 200 K for $HBr^+(A)$ and are nearly independent of the collision energy. The bimodal rotational distributions suggest that at least two processes contribute to formation of these ions. The model potential surface calculated for He*(Li) + HCl as the entrance channel is nearly isotropic and shows a shallow well of about 20 meV, whereas the surface for He + $HCl^+(A)$ as the exit channel is anisotropic and shows a deep minimum of 250 meV in the He−H−Cl collinear direction. Dynamical effects of the anisotropic attractive structure in the exit surface are proposed to account for the observed results.

1. Introduction

Penning ionization is a main decay channel for the collisions between helium metastable atoms (R*) and simple molecules (M). It is now understood to occur through the formation of a quasimolecule (RM*) that autoionizes, producing a free electron and a RM^+ ion. Because the RM^+ ion is unstable, it dissociates into a helium atom and a molecular ion. Molecular ions formed in an electronically excited state (M^{+}*) often fluoresce. Penning ionization of HCl and HBr has been investigated by using two methods, Penning ionization electron spectroscopy (PIES) and Penning ionization optical spectroscopy (PIOS).

Richardson and Setser[1] were the first to use PIOS to study the $He(2^3S)$ + HCl/HBr reactions in a flowing afterglow (FA) apparatus. They found non-Franck−Condon (FC) vibrational distributions for the product $HCl^+(A)$ and $HBr^+(A)$ ions. The distributions were also different from the PIES results[2−5] and shifted to lower vibrational levels. To clarify the origin of the discrepancy between PIOS and PIES data, Martin and coworkers[6] have investigated the $He(2^3S)$ + HCl/HBr reactions under single collision conditions using a crossed molecular beam apparatus. Because they obtained nearly FC vibrational distribution, the deviation of the FA-PIOS data from the PIES data was attributed to vibrational relaxation by collisions with He buffer gas or secondary reactions. Obase et al.[7] subsequently have measured nascent vibrational and rotational distributions of $HCl^+(A)$ and $HBr^+(A)$ resulting from the $He(2^3S)$+HCl/HBr reactions using a low-pressure experimental apparatus. They found that the vibrational distribution of $HCl^+(A)$ agrees well with the PIES data, which shows an FC distribution, although the vibrational distribution of $HBr^+(A)$ is more deexcited than the PIES data, shifting to lower vibrational levels relative to FCF for ionization. They concluded that the energy transfer between the vibration and translation occurs not only at the entrance channel for the $He(2^3S)$ + HCl system but at both the entrance and the exit channels for the $He(2^3S)$ + HBr system. Nevertheless, previous discussions on the reaction dynamics for $He(2^3S)$ Penning ionization of HCl and HBr have tended to be rather qualitative.

In this work, we have measured the emission cross sections (σ_{em}) in the 200−600 nm region resulting from the collision of $He(2^3S)$ with HCl and HBr using a crossed-beam apparatus and examined the nascent rotational and vibrational distributions of $HCl^+(A)$ and $HBr^+(A)$ in the collision energy range of 120−200 meV. The main purpose of the present paper is to describe the mechanism for the Penning ionization based on the internal distributions of the product ions and the potential surfaces calculated for both the entrance and exit channels.

2. Experimental Section

The apparatus and experimental details concerning the fluorescence measurement were reported previously.[8,9] In brief, $He(2^3S, 2^1S)$ atoms are produced with a nozzle discharge source[10] and skimmed into a collision chamber; the singlet component of the total He* flux was estimated to be about 10%. Target gases flowed out to the collision chamber forming an effusive molecular beam through a multicapillary array. Under typical stable operating conditions, the discharge current was 10−30 mA, the voltage was 400−750 V, and the pressure of residual gas at the collision chamber as measured by an ionization vacuum gauge was less than 2.7 mPa. The gases of HCl (Takachiho, 99.999% in stated purity), HBr (Tri-Chemical

* To whom correspondence should be addressed. E-mail: itok-pc@scux.sc.niigata-u.ac.jp.

10.1021/jp014104n CCC: $22.00
Published on Web 06/04/2002

Lab., 99.9995%), and He(Nihon-Sanso, 99.9999%) were used without further purification.

The velocity distribution of the He* beam measured by a time-of-flight method in the separate experiment was nearly represented by a Gaussian function. The root-mean-square velocity (v_A) of the He* beam was found to depend only on the discharge power at the beam source.[9] By using the relative velocity averaged over the velocities of He* atoms and the target molecules, the collision energy dependence of σ_{em} was obtained by converting the function of v_A into that of the relative collision energy (E_R) with the relation between E_R and the reduced mass (μ) of the He + target system:

$$E_R = \mu(v_A 2 + 3kT/m)/2 \qquad (1)$$

where T is the temperature (300 K) and m is the mass of the target molecule. In the fluorescence measurement, we did not use the velocity-selected He* beam because of the weak fluorescence intensity. Thus, applying the fact that v_A increases with the discharge power, we controlled the kinetic energy of the He* beam by varying the discharge power. The kinetic energy distribution of the He* beam was estimated to be 40 meV (hwhm) at $E_R = 120$ and 80 meV at 200 meV. We should mention that the collision energy dependences of the internal distribution for the product ions were measured using the He* beam with a relatively broad collision energy.

The fluorescence resulting from the collision of $He(2^3S)$ with the target molecules was observed in a direction perpendicular to both the molecular and He* beams. The fluorescence focused onto the entrance slit of a SPEX 1704 monochromator was detected by a CCD detector (PI, LN/CCD1100PB) for the measurement of the high-resolution spectrum or a Hamamatsu R585 photomultiplier for other measurements. The σ_{em} for the fluorescence produced by collision of $He(2^3S)$ was evaluated by comparing its emission intensity with that of the $N_2^+(B^2\Sigma_u^+ - X^2\Sigma_g^+)$ band produced by the following Penning ionization:

$$He(2^3S) + N_2 \rightarrow N_2^+(B^2\Sigma_u^+) + He + e^- \qquad (2)$$

We adopted a σ_{em} value of $(3.2 \pm 0.3) \times 10^{-20}$ m^2 for reaction 2 at an E_R of 140 meV; this value was estimated from Figure 5 in ref 11. The total emission intensity of the $N_2^+(B-X)$ system was derived from the intensities of the 0−0 and 1−0 bands by using the scaling factors calculated by Comes and Speier.[12] The density and spatial distribution of N_2 and the target molecules at the collision region were calibrated, and the relative sensitivity of the total photon-detection system was calibrated with a deuterium lamp in the 200−310 nm range and a halogen lamp in the 310−600 nm range.

3. Theoretical Methods

To discuss the observed results concerning the collision energy dependence of the σ_{em}'s for the $HCl^+(A-X)$ band and the rotational and vibrational distributions for $HCl^+(A)$, the interaction potentials for a $He(2^3S)$ atom approaching a hydrogen atom or chlorine atom along several directions were calculated for both the entrance and exit channels using ab initio molecular orbital (MO) methods.

For the $He(2^3S) + HCl(X^1\Sigma^+)$ system as the entrance channel, there are difficulties associated with calculating the excited states. Consequently, a $Li(2^2S)$ atom was used in place of $He(2^3S)$ in the present study because of the well-known resemblance between $He(2^3S)$ and $Li(2^2S)$.[13,14] The interaction potentials between a $Li(2^2S)$ atom and HCl were calculated using the Gaussian 98 program package[15] in the Møller−Plesset perturbation method (MP2) with the frozen-core approximation. The standard 6-31++G(3df, 3p) basis set was used. All calculations were performed with personal computers.

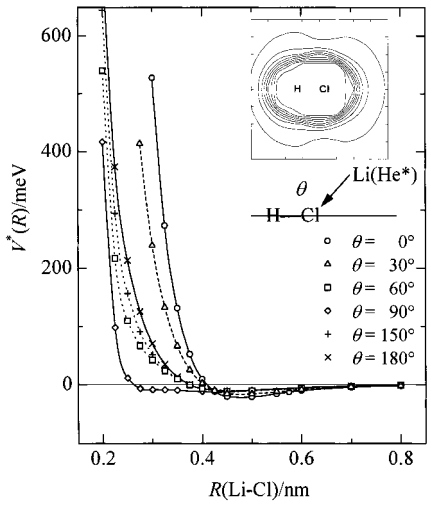

Figure 1. Model potential curves $V^*(R)$ for $HCl(X^1\Sigma^+)$-He*($Li(2^2S)$) as a function of the Li−Cl distance; θ represents the H−Cl−Li angle between the molecular axis and the Li−Cl direction.

To draw the potential energy surfaces correlated with $He(^1S) + HCl^+(X^2\Pi)$ and $He(^1S) + HCl^+(A^2\Sigma^+)$, we performed multireference configuration interaction (MRCI) calculations. The basis set used in this work was the triple-ζ atomic natural orbital (ANO) basis set of Widmark et al.[16] The reference configuration state functions (CSFs) in the MRCI calculations consisted of a full valence complete active space, which included all molecular orbitals (MOs) arising from the valence atomic s, p (Cl), and s (H, He) orbitals (9 electrons in 6 orbitals). From the reference functions, all of the single and double excitations were generated, with the exception of the frozen-core orbitals, 1s, 2s, and 2p (Cl). The total number of the configurations of the final internally contracted MRCI calculations was about 480 000. The MOs for the MRCI calculations were taken from the natural orbitals determined by the state-averaged complete active space self-consistent field (CASSCF) calculations for two A' and a A'' states, using the same active space. All calculations were carried out with the MOLPRO program package.[17] The computer was an SGI Origin 2800 owned by the Research Center for Computational Science at Okazaki.

4. Results and Discussion

4.1. Potential Energy Surfaces for the Entrance and Exit Channels. Figure 1 shows the potential curve $V^*(R)$ for the $HCl(X^1\Sigma^+)$ + He*($Li(2^2S)$) system as the entrance channel obtained from the model potential calculation; R is the distance between the Li atom and the Cl atom when the Li atom approaches along several directions. The surface V^* for the entrance channel is nearly isotropic and shows a shallow well of 20−30 meV, which may originate in the dispersion force. The repulsive wall at $\theta = 90°$ is steeper than that for the collinear direction.

Figure 2 shows the potential curve $V^+(R)$ for the $HCl^+(A^2\Sigma^+)$ + $He(^1S)$ system as the exit channel; R is the distance between the He atom and the Cl atom when the He atom approaches along several directions. The V^+ surface for the exit channel is extremely anisotropic and has deep minima in the collinear direction. The minimum at $\theta = 0°$ (i.e., the He−H−Cl collinear direction) is 250 meV, whereas the well at $\theta = 90°$ is only 20

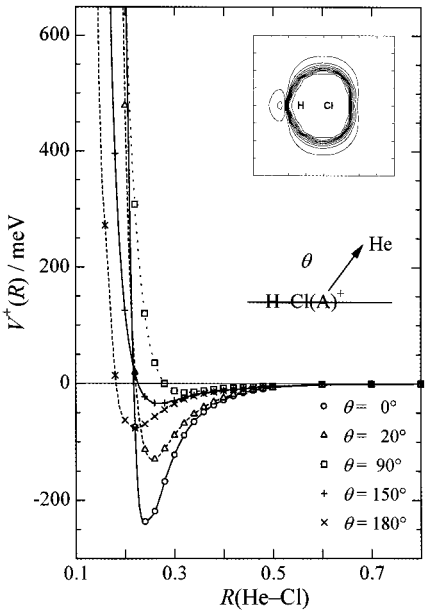

Figure 2. Potential curves $V^+(R)$ for $HCl^+(A^2\Sigma^+)$-He(^{1}S) as a function of the He−Cl distance; θ represents the H−Cl−He angle between the molecular axis and the He−Cl direction.

TABLE 1: σ_{em} Values for the Species Produced by the He(2^3S) + HCl Collision Measured at E_R = 160 MeV

species	λ/nm	$\sigma_{em}/(10^{-20}$ m$^2)$
$HCl^+(A^2\Sigma^+-X^2\Pi)$	270−500	$3.7_4 \pm 0.5$
H_β	486	0.144 ± 0.026
H_γ	434	0.068 ± 0.012
H_δ	411	0.025 ± 0.007
total	270−500	$3.9_8 \pm 0.5$

meV. The repulsive parts of the V^+ surface are harder than those of the surface V^*. For all cases, the bond length of H−Cl was fixed at 127.35 pm, which was the optimized value for $HCl(X^1\Sigma^+)$. On the contrary, the potential surface for the $HCl^+(X^2\Pi)$ + He(^{1}S) system is nearly isotropic and has a shallow well of 20−30 meV around R = 300 pm.

4.2. Emission Cross Sections and Their Collision Energy Dependences. The emission in the 200−660 nm region produced by the collision of He(2^3S) with HCl or HBr was assigned to the hydrogen Balmer series and the $A^2\Sigma^+$-$X^2\Pi$ band for HCl^+ or HBr^+. The intensities for atomic chlorine and bromine were negligible. Table 1 summarizes the σ_{em} values for the several species observed from the collision of He(2^3S) with HCl. The total σ_{em} for HCl in the 200−600 nm region was determined to be 4×10^{-20} m^2. Nevertheless, this value seems to be too small compared with the total quenching cross section of He(2^3S), 62×10^{-20} m^2, as measured by Bush et al.[18] The He + HCl^+(A) products may decay to the He + HCl^+(X) state with radiationless transitions. This possibility will be discussed in section 4.4. We did not measure the σ_{em} value for HBr because of the serious adsorption on the wall of the gas-introducing line.

To investigate the mechanism for formation of excited states, we measured the dependence of σ_{em} values on the collision energy. If the attractive part of the interaction potential $V^*(R)$ between He(2^3S) and the target molecule is described by

$$V^*(R) = -C_s/R^s \tag{3}$$

the cross section is represented by[19]

$$\sigma(E_R) \propto E_R^{-2/s} \tag{4}$$

When the collision energy is very low, the cross section for the Penning ionization decreases with increasing collision energy, eventually reaching a minimum.[20] As the collision energy is further increased, the cross section reaches a maximum and then decreases again at higher energies. Under orbiting approximation, this result can be applied to the formation of the excited neutral fragments produced from neutral excitation.

In this study, the kinetic energy dependence of the σ_{em} value was measured for the 0−0 band of the A−X system of HCl^+ and HBr^+ and the hydrogen Balmer β line (H_β). Figure 3 shows the dependences for the HCl^+(A−X) and HBr^+(A−X) bands and the hydrogen Balmer β line. All emissions were found to decrease with increasing E_R; the s value estimated from the slopes is 7−12. This result indicates that either an attractive potential governs the formation of the emitters or the collision reaches to the high speed limit. The potential curves calculated for the entrance channel show only a shallow well of about 20 meV for all directions. Thus, we prefer the latter case for the He(2^3S) + HCl/HBr collision despite the rather low collision energies.

4.3. Vibrational Populations for HCl^+(A) and HBr^+(A). To evaluate the collision-energy dependence of the vibrational populations for HCl^+(A) and HBr^+(A), the intensity ratios of several bands of the A−X emission were measured: the 0−0, 2−0, and 3−0 bands for HCl^+ and the 0−0 and 1−0 bands of the $\Omega = {}^3/_2$ component for HBr^+.

If the radiationless processes do not occur within the lifetime, the population of a (v', N') state is proportional to its photoemission intensity. The emission intensity of a transition from the (v', N') state to a (v'', N'') state is represented by

$$I_{v''N''}^{v'N'} = \epsilon_{v''N''}^{v'N'} \nu^3 S_{N'N''} q_{v'v''} R_e^2(\bar{r}_{v'v''}) P_{v'}(N')/(2N'+1) \tag{5}$$

where $\epsilon_{v''N''}^{v'N'}$ is the efficiency of the photon detection system, ν is the transition frequency, $S_{N'N''}$ is the rotational line strength, $q_{v'v''}$ is the FC factor, R_e is the electronic transition moment, $\bar{r}_{v'v''}$ is the r centroid, and $P_{v'}(N')$ is the formation rate of the (v', N') state. For low resolution spectra, the ratio of the population for the v' state relative to that for the v' = 0 state derived from the integrated intensities of the 0−0 and v'-v'' bands are

$$\frac{P_{v'}}{P_0} = \frac{I_{v'v''}}{I_{00}} \frac{(\lambda_{v'v''}/\lambda_{00})^3}{(q_{v'v''}/q_{00})[R_e(\bar{r}_{v'v''})^2/R_e(\bar{r}_{00})^2]} = \frac{I_{v'v''}}{I_{00}} F_{v'0} \tag{6}$$

where λ is the transition wavelength. The molecular constants are put into a conversion factor $F_{v'0}$ for convenience.

Haugh et al.[21] tabulated the $q_{v'v''}$ and $\bar{r}_{v'v''}$, and illustrated the r-centroid dependence of the transition moment for the HCl^+-(A−X) and HBr^+(A−X) systems assuming Morse potentials. Later, Ibuki et al.[22] recalculated the dependence of the electronic transition moments on the r centroid for the HCl^+ based on their photoionization and ab initio results by using the $q_{v'v''}$ and $\bar{r}_{v'v''}$ given by Haugh et al.[21] For HBr^+(A), Obase et al.[23] recalculated the Morse potential FC factors and r centroids by using the constants given by Lebreton.[24] The electronic transition moments thus reported strongly depend on the internuclear distance. Furthermore, there are significant discrepancies among the dependences on the r centroid. Nevertheless, it was found that the $F_{v'0}$ factors calculated from these data agree within 6% each other; the $F_{v'0}$ factor is estimated to be 0.73 ± 0.02 for v' = 2 and 1.13 ± 0.03 for v' =3 of HCl^+(A) and 0.55 ± 0.04 for v' =1 of HBr^+(A).

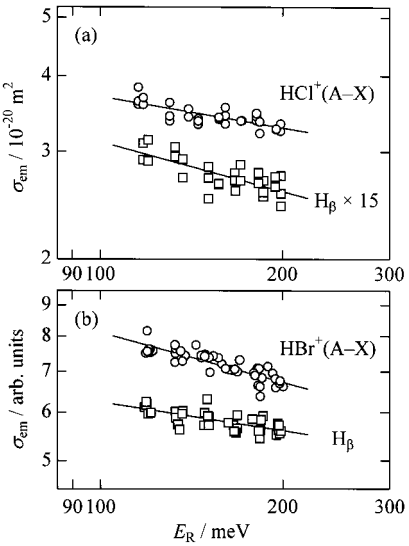

Figure 3. $\log(\sigma_{em})$ vs $\log(E_R)$ plots for (a) the $HCl^+(A-X)$ band and the H_β line from HCl and (b) the $HBr^+(A-X)$ band and the H_β line from HBr.

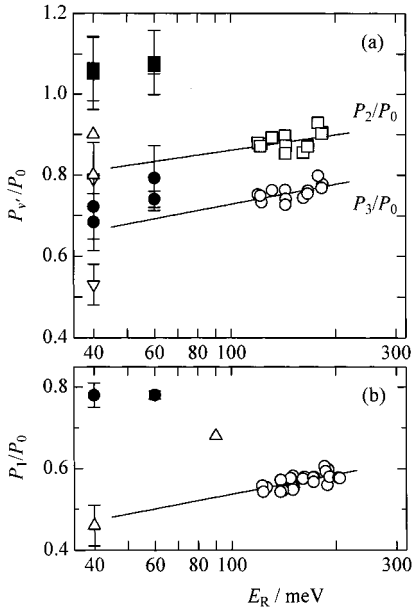

Figure 4. Relative vibrational populations of (a) P_2/P_0 and P_3/P_0 for $HCl^+(A)$ and (b) P_2/P_0 for $HBr^+(A)$. The filled and open symbols represent PIES and PIOS data, respectively; (□, ○) this work, (●, ■) refs 2−5, (▽, △) refs 6 and 7.

Figure 4 shows P_2/P_0 and P_3/P_0 for $HCl^+(A)$ and P_1/P_0 for $HBr^+(A)$ in the $E_R = 120-200$ meV range. All ratios increase with E_R. The ratios extrapolated to the thermal region agree reasonably with the PIOS data but are shifted to lower than the PIES data. The discrepancy of P_1/P_0 for $HBr^+(A)$ between the PIOS and PIES data may be partly caused by predissociation[25] as described minutely below. Nevertheless, the correction of the PIOS data for predissociation was estimated to be 5% at the most. The positive slope of the ratios observed in this study supports that the discrepancy between the PIES and PIOS data originates in the postcollision interactions between the translational and the vibrational mode of the product ion.[2] Moreover, the slopes for $HCl^+(A)$ are nearly equal to that for P_1/P_0 of $HBr^+(A)$. This indicates that the interactions affect the vibrational distributions of the product ions to the same degree.

4.4. Rotational Populations for $HCl^+(A)$ and $HBr^+(A)$. The observed emission spectra were analyzed by means of a computer simulation to determine the rotational distributions of $HCl^+(A)$ and $HBr^+(A)$. The emission intensity of a transition from the (v', N') state to the (v'', N'') state is represented by eq 5. The transition frequencies for the $HCl^+(A^2\Sigma^+-X^2\Pi)$ band were calculated by the formulas[26] for the rotational energy levels of the X and A states with the revised spectroscopic constants.[27] Those for $HBr^+(A-X)$ were calculated by the spectroscopic constants reported by Lebreton.[24] The line strengths were calculated according to the formula given by Kovács[28] with the spectroscopic data.[24,26] The Hg line at 365 nm was used as a slit function that was convoluted into the rotational lines to calculate the spectral envelope.

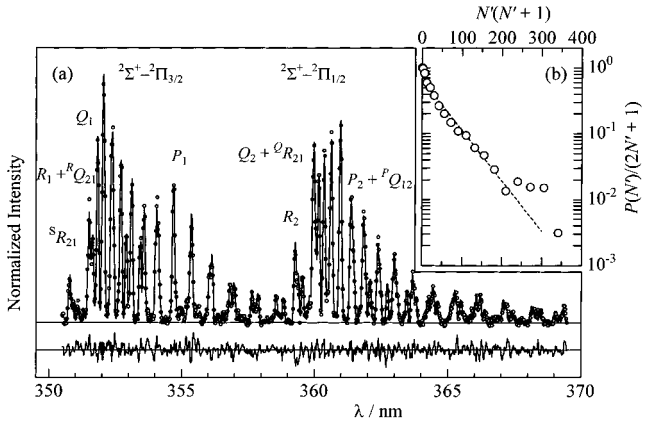

Figure 5. (a) Observed spectrum (○) of the 0−0 band for the HCl^+-(A−X) emission measured at $E_R = 150$ meV with the 0.2 nm fwhm resolution; the upper trace represents the best-fit synthetic spectrum, and the lower is the residual; (b) rotational populations of $HCl^+(A, v' = 0)$. The broken line represents a Boltzmann temperature of 600 K.

Figure 5a shows the observed and synthetic spectra for the 0−0 band of the $HCl^+(A-X)$ emission. In preliminary analysis, it was found that the weak 1−1, 2−1, 3−2, and 4−2 bands were heavily overlapped with the 0−0 band. To evaluate the rotational populations for $HCl^+(A, v' = 0)$, the intensities of these weak bands were treated as fitting parameters in the band-envelope analysis under the assumption that the rotational distributions for the $v' = 1-4$ levels are represented by Boltzmann temperatures; in this analysis, the Boltzmann temperatures for $v' = 1-4$ were fixed at 550, 500, 400, and 350 K, respectively, as observed by Obase et al.[7] The rotational populations obtained for the $HCl^+(A, v' = 0)$ state are shown in Figure 5b. It is obvious that a simple Boltzmann temperature cannot represent the distribution because the plot is not straight. It was found that a double-Boltzmann distribution successfully explains the observed distribution; the best-fitted temperatures are 180 ± 40 and 770 ± 100 K, and the component with the higher temperatures is (72 ± 4)%. Obase et al.[7] reported a value of 600 ± 100 K for the rotational temperature of $HCl^+(A, v' = 0)$. In the present result, the populations for $N' = 0-14$ can be fitted with a Boltzmann temperature of 550−600 K as shown in Figure 5b. Thus, the present data does not contradict the results of Obase et al.

The 0−0 and 1−0 bands for the $HBr^+(A^2\Sigma^+-X^2\Pi_{3/2})$ emission were analyzed by the band envelopes of the single band. Figure 6 shows the observed and synthetic spectra of the 0−0 band, and Figure 7 shows the rotational distributions for the $v' = 0$ and 1 state of $HBr^+(A)$. Because the plot for $v' = 0$ is not straight, the distribution for $v' = 0$ (shown in Figure 7) was analyzed with a double-Boltzmann distribution; the best-fitted temperatures were 240 ± 30 and 1100 ± 150 K, and the component with the higher temperature was (51 ± 4)%. The rotational distributions for the $HBr^+(A)$ state decrease suddenly

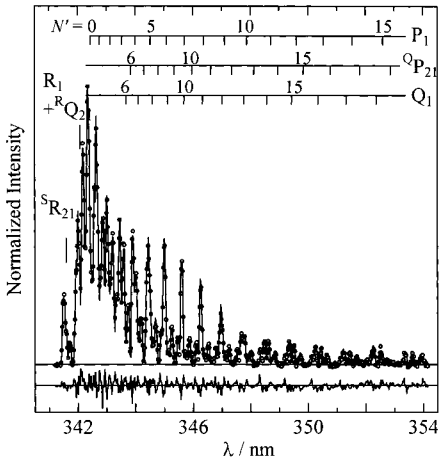

Figure 6. Same as in Figure 5a but for the 0−0 band of the $HBr^+(A-X)$ emission.

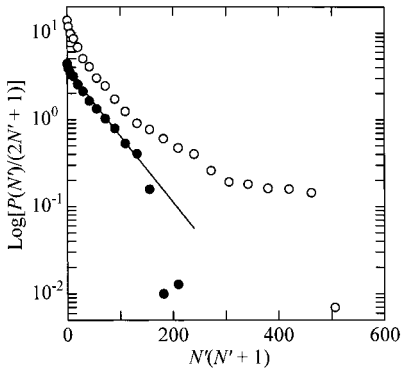

Figure 7. Rotational populations of $HBr^+(A)$ measured at $E_R = 165$ meV; (○) for $v' = 0$ and (●) for $v' = 1$. The solid line for $v' = 1$ represents a temperature of 460 K.

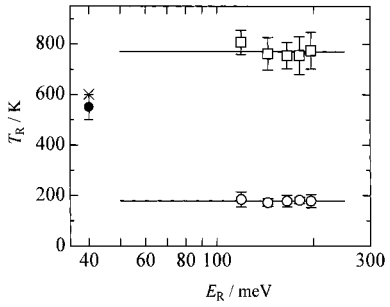

Figure 8. Collision energy dependences of rotational temperatures for $HCl^+(A, v' = 0)$; (○ and □) this work, (●) from ref 7, (×) from ref 5b.

above $N' = 21$ for $v' = 0$ and $N' = 12$ for $v' = 1$ because of predissociation to $H(^2S) + Br^+(^3P)$.[25] For $v' = 1$, the rotational distribution for $N' = 0-11$ can be represented by a single temperature, 460 ± 40 K, probably because the component with higher temperature observed for $v' = 0$ mainly contributes to the populations for $N' \geq 12$.

Figure 8 shows the dependence of rotational temperatures for $v' = 0$ of $HCl^+(A)$, and Figure 9 shows those for $v' = 0$ and 1 of $HBr^+(A)$. The observed temperatures are constant in the 120−200 meV region, whereas the vibrational distribution is enhanced with increasing collision energy. This result suggests that $HCl^+(A)$ and $HBr^+(A)$ are mainly produced by the collinear collision of target molecules and $He(2^3S)$ atoms and the subsequent ejection of a 5σ electron with the H−Cl bonding character.

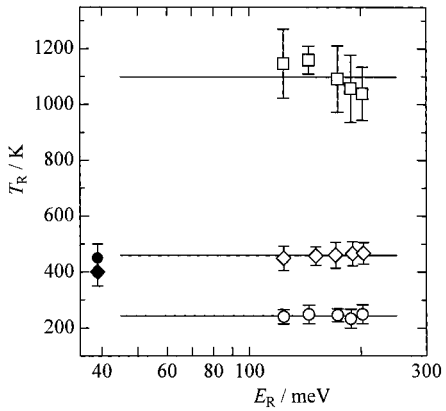

Figure 9. Same as in Figure 8 but for $HBr^+(A, v' = 0, 1)$; (○, □) for $v' = 0$ and (◇) for $v' = 1$, this work and (●) for $v' = 0$ and (◆) for $v' = 1$ from ref 7.

The bimodal rotational distributions of the $v' = 0$ level for $HCl^+(A)$ and $HBr^+(A)$ might originate in one of the following three causes: (A) rotational relaxations or the electronic quenching of the emitter by collisions with helium atoms; (B) the contribution from the $He(2^1S)$ component; and (C) dynamical effects of the structure to exist in the entrance and exit surfaces.

Cause A. The radiative lifetimes for both $HCl^+(A)$ and $HBr^+(A)$ are reported to be about 4 μs.[29] The collision probability of the emitter for the radiative lifetime is estimated to be on the order of 10^{-4} based on the background pressure at the collision region on the assumption of a quenching cross section of 50×10^{-20} m^2. Thus, rotational relaxation or quenching of the emitter is negligible.

Cause B. In this experiment, $He(2^1S)$ was estimated to be 10% in the He* beam. The quenching cross sections for the Penning ionization of HCl were reported to be 62×10^{-20} m^2 for $He(2^3S)$ and 145×10^{-20} m^2 for $He(2^1S)$.[18] The contribution of $He(2^1S)$ to the formation of $HCl^+(A)$ is estimated to be 20%. Obase et al.[7] reported that the $He(2^3S)$ results on effective rotational temperatures for $HCl^+(A, v' = 0-3)$ agree well with the $He(2^1S)$ result reported by de Vries et al.[5b] This fact suggests that the differences in the reactions of $He(2^3S)$ and $He(2^1S)$ with HCl do not affect the Penning ionization dynamics for the formation of $HCl^+(A)$. This consideration may be applied to the formations of $HBr^+(A)$.

Cause C. When the Penning ionization occurs, the HCl−He system transfers from the potential surface for the entrance channel (V^*) into that for the exit channel (V^+); the ionization is essentially the Franck−Condon type. The collision energy dependence of the σ_{em} for the $HCl^+(A-X)$ band shows that the repulsive part of the entrance surface has no effect upon the ionization. Thus, the ionizations occur in the attractive region on the inward leg of the trajectory, before the classical turning point (R_C) of the entrance surface; in the $He(2^3S)$−HCl system, R_C is estimated to be 0.34 nm for $\theta = 0°$, 0.22 nm for $\theta = 90°$, and 0.27 nm for $\theta = 180°$ (see Figure 1). The surface of the exit channel, $HCl^+(A^2\Sigma^+) + He(1^1S)$, has a deep well of about 250 meV at $R(Cl-He) = 0.24$ nm for $\theta = 0°$, whereas the surface has only a shallow well of 20 meV for $\theta = 90°$ (see Figure 2).

In the case that the transfer to the exit channel occurs at attractive regions in a direction perpendicular to the molecular axis, the ionizations deposit the $He + HCl^+(A)$ products in the slightly attractive region maintaining the initial kinetic energy because the two surfaces are very similar in the vicinity of that direction. The products feel a deep well in the direction of $\theta =$

0° and can gain the torque that deforms the conformation from bend to linear. Consequently, the products in some trajectories should be rotationally excited. This dynamical effect of the anisotropic attractive structure in the exit surface may produce the rotationally hot $HCl^+(A)$. This $T \rightarrow R$ energy transfer will be source for the major component of $HCl^+(A)$ with higher temperature.

In the other case that the ionization occurs at attractive regions in the collinear direction, especially from the hydrogen atom side, the ionizations deposit the products on the deep attractive surface. The $HCl^+(A)$ + He products with reduced energy in a relative translation would suffer a mild collision with the hard repulsive wall and then depart from each other maintaining the initial angular momentum. Little energy would be transferred to rotation of $HCl^+(A)$. This mechanism, which produces the rotationally cold $HCl^+(A)$ seems to be minor because the area with deep well is not so large.

A less likely mechanistic possibility for production of the bimodal rotational distributions arises if the $HCl^+(A^2\Sigma^+)$ + He product transfers into the $HCl^+(X^2\Pi)$ + He surface by rotational coupling. The magnitude of the rotational coupling is approximated by $b\upsilon/R^2$,[30] where b is the impact parameter, υ is the relative velocity, and R is the distance between HCl^+ and He. Accordingly, the probability of the transfer becomes large around the classical turning point and increases with the impact parameter within the range that the system can approach to the classical turning point. When the total angular momentum of the system is small, the coupling is relatively small, and the $HCl^+(A)$ + He products undergo inelastic collisions with the hard repulsive wall with a kinetic energy equal to or smaller than the initial energy. Thus, $HCl^+(A)$ with lower N' may be produced via the coupling between the total angular momentum and the rotational angular momentum of $HCl^+(A)$. When the impact parameter becomes large, the probability of the transfer into the $HCl^+(X)$ + He surface increases by angular coupling. The production of $HCl^+(A)$ with higher N' may be depressed. In the largest b, the rotational coupling should be neglected again. From this consideration, the rotational distribution of $HCl^+(A)$ is expected to have a dip around middle N' values. This radiationless transfer into the $HCl^+(X)$ + He surface might be the cause of the small σ_{em} for the $HCl^+(A-X)$ band.

Bimodal rotational distributions were observed in the $N_2^+(X^2\Sigma^+)$ state produced by the $Ne(2^3P)$ Penning ionization of N_2.[31] The structure in the repulsive wall of the entrance surface makes possible ionizing transitions to two distinct regions of the exit surface resulting in collisions of different elasticity with the repulsive wall of the exit surface. The initial repulsive rise in the entrance surface is directly over the well of the exit surface, and the $N_2^+(X)-Ne$ products with reduced energy in relative translation would suffer a mild collision with the repulsive wall. Little energy would be directed into rotation of the $N_2^+(X)$ state. On the other hand, the secondary repulsive rise is over the repulsive wall of the exit surface, and the products undergo a half-collision with a greater kinetic energy. The inelasticity of collisions would produce the rotationally hotter products. The bimodal distributions of both the $Ne(2^3P)-N_2$ and the $He(2^3S)-HCl$ system are governed by differences in entrance potentials and the associated exit potentials around arrival positions. However, unlike the $Ne(2^3P)-N_2$ system, the present system exhibits no evidence of repulsive interaction on the entrance channel given the kinetic energy dependence.

5. Conclusions

$He(2^3S)$ Penning ionization of HCl and HBr has been studied in the collision energy range of 120−200 meV. The σ_{em}'s for the 0−0 band of the $HCl^+(A-X)$ and $HBr^+(A-X)$ transitions decrease with increasing the collision energy. This indicates that the repulsive part of the entrance surface is ineffective on the ionization dynamics. The vibrational distributions of $HCl^+(A)$ and $HBr^+(A)$ are enhanced with increasing collision energy, whereas the rotational distributions of $HCl^+(A, \upsilon' = 0)$ and $HBr^+(A, \upsilon' = 0, 1)$ are independent of the collision energy. This trend suggests that the Penning ionization occurs mainly by the collinear collision. The detailed analysis of the rotational distribution shows a bimodal distribution of the $\upsilon' = 0$ level for $HCl^+(A)$ and $HBr^+(A)$; the component with higher temperature is 70% for $HCl^+(A)$ and 50% for $HBr^+(A)$. The major components with higher temperature seem to be originated in the dynamical effect of $T \rightarrow R$ energy transfer based on the anisotropic attractive surface of the exit channel, whereas the mild collision with the repulsive wall of the exit surface may produce the rotationally cold ion. We are currently calculating the theoretical populations of the $HCl^+(A)$ state based on the more accurate potential surfaces of the entrance and exit channels.

Acknowledgment. This work was partly supported by a Grand-in-Aid for Scientific Research from the Japanese Ministry of Education, Science, Sports, and Culture. S.N. was also supported by the project "Computational Chemistry of Molecules in Atmospheric Environment" of the Research and Development Applying Advanced Computational Science and Technology program of the Japan Science and Technology Corporation.

References and Notes

(1) (a) Richardson, W. C.; Setser, D. W.; Albritton, D. L.; Schmeltekopf, A. L. *Chem. Phys. Lett.* **1971**, *12*, 349. (b) Richardson, W. C.; Setser, D. W. *J. Chem. Phys.* **1973**, *58*, 1809.

(2) Hotop, H.; Hubler, G.; Kaufhold, L. *Int. J. Mass Spectrom. Ion Phys.* **1975**, *17*, 163.

(3) Cermak, V. J. *Electron Spectrosc. Relat. Phenom.* **1976**, *8*, 325.

(4) Brion, C. E.; Crowley, P. *J. Electron Spectrosc. Relat. Phenom.* **1977**, *11*, 399.

(5) (a) Yencha, A. J.; Ganz, J.; Ruf, M.-W.; Hotop, H. *Z. Phys.* **1989**, *D14*, 57. (b) Yencha, A. J.; Ruf, M.-W.; Hotop, H. *Z. Phys.* **1991**, *D21*, 113.

(6) (a) Tyndall, G. W.; de Vries, M. S.; Martin, R. M. *Chem. Phys. Lett.* **1984**, *110*, 400. (b) de Vries, M. S.; Tyndall, G. W.; Martin, R. M. *J. Chem. Phys.* **1984**, *80*, 1366.

(7) Obase, H.; Tsuji, M.; Nishimura, Y. *J. Chem. Phys.* **1987**, *87*, 2695.

(8) Tokue, I.; Kudo, T.; Ito, Y. *Chem. Phys. Lett.* **1992**, *199*, 435.

(9) Tokue, I.; Sakai, Y.; Yamasaki, K. *J. Chem. Phys.* **1997**, *106*, 4491.

(10) Ohno, K.; Takami, T.; Mitsuke, K.; Ishida, T. *J. Chem. Phys.* **1991**, *94* 2675 and references therein.

(11) Sanders, R. A.; Schweid, A. N.; Weiss, M.; Muschlitz, E. E., Jr. *J. Chem. Phys.* **1976**, *65*, 2700.

(12) Comes, F. J.; Speier, F. *Chem. Phys. Lett.* **1969**, *4*, 13.

(13) (a) Hotop, H. *Radiat. Res.* **1974**, *59*, 379. (b) Niehaus, A. *Adv. Chem. Phys.* **1981**, *45*, 399. (c) Haberland, H.; Lee, Y. T.; Siska, P. E. *Adv. Chem. Phys.* **1981**, *45*, 487.

(14) Ohno, K.; Sunada, S. *Proc. Indian Acad. Sci.* **1994**, *106*, 327.

(15) Frisch, M. J.; Trucks, G. W.; Schlegel, H. B.; Scuseria, G. E.; Robb, M. A.; Cheeseman, J. R.; Zakrzewski, V. G.; Montgomery, J. A., Jr.; Stratmann, R. E.; Burant, J. C.; Dapprich, S.; Millam, J. M.; Daniels, A. D.; Kudin, K. N.; Strain, M. C.; Farkas, O.; Tomasi, J.; Barone, V.; Cossi, M.; Cammi, R.; Mennucci, B.; Pomelli, C.; Adamo, C.; Clifford, S.; Ochterski, J.; Petersson, G. A.; Ayala, P. Y.; Cui, Q.; Morokuma, K.; Malick, D. K.; Rabuck, A. D.; Raghavachari, K.; Foresman, J. B.; Cioslowski, J.; Ortiz, J. V.; Stefanov, B. B.; Liu, G.; Liashenko, A.; Piskorz, P.; Komaromi, I.; Gomperts, R.; Martin, R. L.; Fox, D. J.; Keith, T.; Al-Laham, M. A.; Peng, C. Y.; Nanayakkara, A.; Gonzalez, C.; Challacombe, M.; Gill, P. M. W.; Johnson, B. G.; Chen, W.; Wong, M. W.; Andres, J. L.; Head-Gordon, M.; Replogle, E. S.; Pople, J. A. *Gaussian 98*, revision A.9; Gaussian, Inc.: Pittsburgh, PA, 1998.

(16) (a) Widmark, P. O.; Malmqvist, P. A.; Roos, B. *Theor. Chim. Acta* **1990**, *77*, 291. (b) Widmark, P. O.; Persson, B. J.; Roos, B. *Theor. Chim. Acta* **1991**, *79*, 419.

(17) MOLPRO is a package of ab initio programs written by Werner, H.-J.; Knowles, P. J. with contributions from Amos, R. D.; Berning, A.; Cooper, D. L.; Deegan, M. J. O.; Dobbyn, A. J.; Eckert, F.; Hampel, C.; Leininger, T.; Lindh, R.; Lloyd, A. W.; Meyer, W.; Mura, M. E.; Nicklass, A.; Palmieri, P.; Peterson, K.; Pitzer, R.; Pulay, P.; Rauhut, G.; Schütz, M.; Stoll, H.; Stone, A. J.; Thorsteinsson, T.

(18) Bush, Y. A.; McFarland, D. L.; Albritton, D. L.; Schmeltekopf, A. L. *J. Chem. Phys.* **1973**, *58*, 4020.

(19) Niehaus, A. *Adv. Chem. Phys.* **1981**, *45*, 399 and references therein.

(20) Olson, R. E. *Phys. Rev. A* **1972**, *6*, 1031.

(21) Haugh, M. J.; Schneider, B. S.; Smith, A. L. *J. Mol. Spectrosc.* **1974**, *51*, 123.

(22) Ibuki, T.; Sato, N.; Iwata, S. *J. Chem. Phys.* **1983**, *79*, 4805.

(23) Obase, H.; Tsuji, M.; Nishimura, Y. *Chem. Phys.* **1985**, *99*, 111.

(24) Lebreton, J. *J. Chim. Phys.* **1973**, *70*, 1188.

(25) Haugh, M. J.; Bayes, K. D. *J. Phys. Chem.* **1971**, *75*, 1472.

(26) Sheasley, W. D.; Mathews, C. W. *J. Mol. Spectrosc.* **1973**, *47*, 420.

(27) Saenger, K. L.; Zare, R. N. *J. Mol. Spectrosc.* **1976**, *61*, 216.

(28) Kovács, I. *Rotational Structure in the Spectra of Diatomic Molecules*; Hilger: London, 1969.

(29) (a) Möhlmann, G. R.; de Heer, F. J. *Chem. Phys.* **1976**, *17*, 147. (b) Möhlmann, G. R.; Bhutani, K. K.; de Heer, F. J. *Chem. Phys.* **1977**, *21*, 127. (c) Martner, C. C.; Pfaff, J.; Rosenbaum, N. H.; O'Keefe, A.; Saykally, R. J. *J. Chem. Phys.* **1983**, *78*, 7073.

(30) Bransden, B. H. *Atomic Collision Theory*; Benjamin/Cummings: London, 1983; p 352.

(31) (a) Sonnenfroh, D. M.; Leone, S. *J. Chem. Phys.* **1987**, *87*, 5041. (b) Sonnenfroh, D. M.; Leone, S. R. *Int. J. Mass Spectrosc. Ion Process.* **1987**, *80*, 63.